Dynamic neural and glial responses of a head-specific model for traumatic brain injury in *Drosophila*

Janani Saikumar[a], China N. Byrns[b], Matthew Hemphill[c], David F. Meaney[c,d], and Nancy M. Bonini[a,b,1]

[a]Department of Biology, University of Pennsylvania, Philadelphia, PA 19104; [b]Neuroscience Graduate Group, Perelman School of Medicine, University of Pennsylvania, Philadelphia, PA 19104; [c]Department of Bioengineering, University of Pennsylvania, Philadelphia, PA 19104; and [d]Department of Neurosurgery, University of Pennsylvania, Philadelphia, PA 19104

Contributed by Nancy M. Bonini, April 29, 2020 (sent for review March 2, 2020; reviewed by Stephen L. Helfand and Doris Kretzschmar)

Traumatic brain injury (TBI) is the strongest environmental risk factor for the accelerated development of neurodegenerative diseases. There are currently no therapeutics to address this due to lack of insight into mechanisms of injury progression, which are challenging to study in mammalian models. Here, we have developed and extensively characterized a head-specific approach to TBI in *Drosophila*, a powerful genetic system that shares many conserved genes and pathways with humans. The *Drosophila* TBI (dTBI) device inflicts mild, moderate, or severe brain trauma by precise compression of the head using a piezoelectric actuator. Head-injured animals display features characteristic of mammalian TBI, including severity-dependent ataxia, life span reduction, and brain degeneration. Severe dTBI is associated with cognitive decline and transient glial dysfunction, and stimulates antioxidant, proteasome, and chaperone activity. Moreover, genetic or environmental augmentation of the stress response protects from severe dTBI-induced brain degeneration and life span deficits. Together, these findings present a tunable, head-specific approach for TBI in *Drosophila* that recapitulates mammalian injury phenotypes and underscores the ability of the stress response to mitigate TBI-induced brain degeneration.

neural injury | glial response | stress response | traumatic brain injury | *Drosophila*

Traumatic brain injury (TBI) has a worldwide incidence rate of 69 million new cases each year and is the leading cause of all injury-related deaths (1, 2). Neural injury is caused by rapid acceleration forces that damage axons, glia, and blood vessels (3, 4). This primary mechanical damage causes breaching of the blood–brain barrier (BBB) (4), dysregulated ion flux, and glutamate excitotoxicity (5), leading to excessive accumulation of intracellular calcium (6). The resulting molecular cascades include oxidative stress, inflammation, and cell death pathways leading to neural loss (6–11). A major long-term consequence of TBI is the accelerated development of cognitive dysfunction and neurodegenerative diseases like chronic traumatic encephalopathy (CTE), Alzheimer's disease, and amyotrophic lateral sclerosis (10, 11).

Despite decades of research, clinical trials on neuroprotective agents for TBI have been singularly unsuccessful (12). One of the contributing factors is an incomplete understanding of key long-term aspects of secondary injury that continue to develop years after the initial TBI. In rodent models, large-scale experiments such as those exploring the long-term consequences of injury are unfeasible. Precise genetic manipulations to dissect the molecular mechanisms that underlie the heterogenous TBI pathophysiology are challenging and time-consuming. Thus, there is a niche for models of TBI in simpler systems where rapid, high-throughput genetic or pharmacological screens can be conducted, and genetic manipulations performed with ease to gain a better understanding of the molecular responses.

Drosophila melanogaster has been instrumental in elucidating the mechanisms of a wide range of biological processes with application to human disease (13, 14), including neurodegenerative disorders. Powerful genetic tool kits can be used for spatial and temporal manipulation of target genes, allowing for rapid identification of disease modifiers through large-scale genome-wide screens (15, 16). Existing models of TBI in *Drosophila* confine flies to plastic vials and cause mechanical trauma to the whole fly body either by a spring-based mechanism (17, 18) or a bead mill homogenizer (19). Although these studies have helped establish *Drosophila* as a platform for studying TBI, collateral damage caused to tissues other than the head can confound observations and obscure brain-specific injury signatures. The primary injuries can be inconsistent between individual animals, leading to heterogeneity in the population. One head-specific model of injury has been described (20) although it is not extensively characterized and may be challenging for high-throughput applications.

We present a paradigm for inflicting traumatic injury selectively to the fly head using a piezoelectric actuator that rapidly and precisely compresses the head against a metal plate. The extent of head compression determines the severity of brain injury, allowing three thresholds of injury: mild, moderate, and severe. We comprehensively characterize the response of injured animals at the behavioral, histological, and molecular levels over time. We demonstrate that an intervention in the endogenous stress response using genetic and environmental manipulations prior to injury mitigates the deleterious outcomes of TBI. These data present a *Drosophila* injury paradigm that recapitulates key

Significance

***Drosophila melanogaster* is a powerful genetic model organism, facilitating major discoveries in the mechanisms of neurological disease and providing the framework for future translational research. We have developed a *Drosophila* model to study traumatic brain injury (TBI)-induced neurodegeneration. The use of *Drosophila* in addition to mammalian models of TBI research is significant, because of the potential to perform large-scale genetic or pharmacological screens, and easy spatial and temporal manipulation of genes. Our model of TBI in *Drosophila* (dTBI) is an advance over current fly models, which confer varying injury to the whole animal rather than the head. The dTBI response is strikingly similar to mammals, indicating that TBI, like genetic human neurodegenerative diseases, can be successfully modeled in *Drosophila*.**

Author contributions: J.S., M.H., D.F.M., and N.M.B. designed research; J.S. performed research; J.S., C.N.B., and N.M.B. analyzed data; M.H. and D.F.M. designed and built the dTBI device; N.M.B. supervised research; and J.S. and N.M.B. wrote the paper.

Reviewers: S.L.H., Brown University; and D.K., Oregon Health and Science University.

The authors declare no competing interest.

Data deposition: The information required to assemble and use the dTBI device is publicly accessible at Protocol Exchange (http://dx.doi.org/10.21203/rs.3.pex-949/v1).

[1]To whom correspondence may be addressed. Email: nbonini@sas.upenn.edu.

This article contains supporting information online at https://www.pnas.org/lookup/suppl/doi:10.1073/pnas.2003909117/-/DCSupplemental.

First published July 1, 2020.

pathophysiological aspects of mammalian TBI, which can facilitate the identification of important molecular mechanisms of protection for the development of therapeutics.

Results

***Drosophila* TBI (dTBI): A Closed Head Model of TBI in *Drosophila*.** We developed a head-specific paradigm of TBI in *Drosophila*, which we refer to as *Drosophila* TBI (dTBI), by building a device to deliver a controlled, reproducible compression to the fly head (*SI Appendix*, Fig. S1*A*). The design relies on the head being positioned between the tip of a piezoelectric actuator and a solid surface. The piezoelectric actuator deflects downward upon the application of voltage, causing the head to be rapidly (within 250 ms) compressed against the solid surface (Movie S1). The timing, speed, and magnitude of deflection are precisely controlled by an Arduino-based microcontroller system that outputs the required voltage to the piezoelectric. Fly collars (21) with custom modifications (*Materials and Methods*) are used to restrain animals, providing the solid surface against which the head is compressed (Fig. 1*A*).

Device calibration consisted of multiple steps to ensure accurate and reproducible head deformation. First, the relationship between the microcontroller output voltage and piezoelectric actuator deflection was measured to verify that the actuator responds linearly (*SI Appendix*, Fig. S1*B*, R^2 = 0.996, root mean squared error (RMSE) = 5.228 μm). Second, the extent of head compression was measured with increasing output voltage, indicating that head compression varied linearly with voltage (Fig. 1*B*, R^2 = 0.996, RMSE = 1.007%). With the current temporal resolution of the camera, each compression event was observed to occur within 300 to 350 ms.

Based on functional characterizations (see below), four severities of head compression were selected for further study and categorized as mild injury (35% compression), moderate (40%), severe (45%), and lethal (55%) (all animals are dead by 7 d postinjury) (Fig. 1*B*). Importantly, the compression did not introduce morphological defects to the cuticle, antennae, or eyes, even at the highest compression level (*SI Appendix*, Fig. S1*D*). Experiments included a sham group of animals that were collared but not hit. To examine potential effects of collaring, a control group of animals that had not been collared was included for select experiments.

Dose-Dependent Neurological Defects following dTBI. We characterized the dTBI response by studying the range of features displayed by injured animals over a 10-d postinjury period. Notably, these features are reflective of the mammalian response to TBI (*Discussion*). All injured animals experienced an immediate and temporary ataxia, during which they were unable to right themselves after being placed on their back. The time required to regain the righting reflex was proportional to the compression severity: Sham animals regained normal posture instantaneously, mildly injured animals took 1 min, while lethally injured animals took almost 5 min to recover (Fig. 1*C*). For up to 30 min after the injury, 90% of moderately and severely injured and 70% of mildly injured animals exhibited a variety of behaviors reflective of incoordination and spontaneous seizures (*SI Appendix*, Fig. S1*E*). These included walking in circles or sideways instead of a straight line, uncontrolled "jumps" across the vial which often

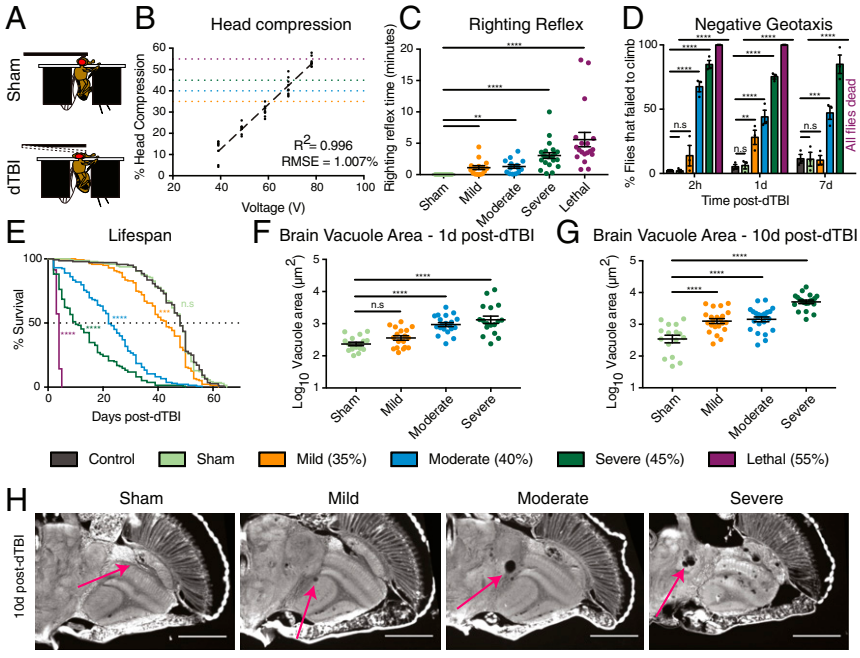

Fig. 1. Development of a head-specific TBI model in *Drosophila*. (*A*) Schematic of the piezoelectric dTBI device. (*B*) Compression of the fly head with the piezoelectric varies linearly with supplied voltage (goodness of fit coefficient of determination 0.996, RMSE = 1.007%). Replicates: 40 V, 50 V, 80 V = eight trials, 60 V, 70 V = nine trials. Dotted lines indicate mild (35%, orange), moderate (40%, blue), severe (45%, green) and lethal (55%, purple) head compression chosen for further studies. (*C*) Righting reflex time (min) increases with greater head compression. Mean ± SEM. Number of animals: Sham, 20; Mild, 15; Moderate, 14; Severe, 22; Lethal, 19. (*D*) dTBI animals show dose-dependent climbing defects within 2 h postinjury that persist till 7 d postinjury. Mean ± SEM, three trials of 20 flies per group. (*E*) Dose-dependent reduction in life span with dTBI. Dotted line indicates median survival. Number of animals: 100 flies per group. (*F*) Severity of brain vacuole formation ($\log_{10}$ of vacuole area [μm^2]) increases with dTBI at 1 d and (*G*) 10 d postinjury. Mean ± SEM. Number of brains scored for 1 d: Sham, 17; Mild, 18; Moderate, 20; Severe, 17. For 10 d: Sham, 16; Mild, 22; Moderate, 23; Severe, 20. (*H*) Representative horizontal paraffin sections showing the increase in the presence of vacuoles (arrows) with increasing dTBI severity at 10 d postinjury. (Scale bars: 100 μm.) Genotypes for all figures: w^{1118} male. Statistics: (*C*) Kruskal–Wallis test with Dunn's correction, (*D*) two-way ANOVA with Dunnett's test, (*E*) log-rank test comparing each group to Control, (*F* and *G*) one-way ANOVA with Dunnett's test. $^{**}P < 0.01$, $^{***}P < 0.001$, $^{****}P < 0.0001$, n.s. not significant.

led to seizure-like twitches (Movie S2). Using a climbing assay to assess locomotor abilities, we found that dTBI caused dose-dependent deficiencies within 2 h that persisted up to at least 7 d for the moderately and severely injured animals (Fig. 1*D*). Two-way ANOVA analysis showed a significant effect of injury condition but no significant effect of time, indicating that the locomotor ability is not recovered after dTBI.

dTBI also caused a reduction in life span for all of the injury severities. Of note, collaring had no effect on survival, with both sham and noncollared control groups having a median life span of 48 d. Median life spans after dTBI were as follows: mild injury 43 d, moderate injury 22 d, severe injury 10 d, and lethal injury 4 d (Fig. 1*E*). The long-term impact of dTBI on health could be seen in the appearance of brain vacuoles, which are a characteristic feature of neurodegeneration in flies (14). Vacuoles appeared by 1 d postinjury with moderate and severe dTBI (Fig. 1*F*). By 5 d postinjury, even the mildly injured brains had vacuoles (*SI Appendix*, Fig. S1*F*). By 10 d, the mild group had 3.7-fold as many vacuoles as the sham, moderate had 4.2-fold, while the severely injured flies had 14.7-fold more (Fig. 1*G*). Vacuoles were found throughout the neuropil and lamina and increased in size and number with injury (Fig. 1*H*). Several severely injured brains had multiple large vacuoles that appeared to coalesce in the neural cell body cortex (*SI Appendix*, Fig. S1*G*). To determine whether the vacuoles preferentially occurred in a particular region of the brain, we analyzed the location of vacuoles in severely injured animals at 10 d (*SI Appendix*, Fig. S1*H*). Vacuoles were most prevalent in the ventral subesophageal ganglion (*SI Appendix*, Fig. S1 *H* and *I*, brown regions), central neuropils (*SI Appendix*, Fig. S1 *H* and *I*, red and blue regions), and optic lobes (*SI Appendix*, Fig. S1 *H* and *I*, purple regions), and were relatively infrequent in the dorsal brain (*SI Appendix*, Fig. S1 *H* and *I*, yellow regions). These sites of vacuolization correspond to the site of the head impact, which is the ventralmost part of the head, just past the antennae (*SI Appendix*, Fig. S1*J*).

TBI is associated with an acute necrotic death response in the brain (22). Sham and severe dTBI brains were therefore assessed at 1 d and 10 d postinjury for permeability to propidium iodide, a widely used marker for necrosis. Injured brains had a significantly higher number of necrotic cells at 1 d, and this difference had subsided by 10 d postinjury (*SI Appendix*, Fig. S1*K*).

An effect of dTBI was the dose-dependent development of an enlarged abdomen within 2 to 3 d of injury (*SI Appendix*, Fig. S2). This effect was associated with only a portion of the animals (~50% in even severe dTBI), and further experiments included both normal and affected animals. Animals that do not have this phenotype and mild dTBI animals, where the effect is minimal, both undergo brain vacuolization, indicating that this does not drive brain degeneration.

Overall, animals subject to the dTBI paradigm reflect a number of neurological consequences of human TBI, including ataxia, locomotor deficits, shortening of life span, necrosis and brain degeneration.

Severe dTBI Animals Have Deficient Memory Acquisition and Cholinergic Neurons. Brain trauma is associated with progressive neurological degeneration, and human epidemiological studies implicate TBI as the biggest environmental risk factor for the development of late-life dementia (11). To investigate whether cognitive impairment was a feature of dTBI, we employed a well-established paradigm of associative learning through courtship conditioning. In this assay, socially naive males that are paired with an unreceptive female will be sexually rejected. The males learn to modify their innate courting behavior and will display decreased courtship when they subsequently encounter a receptive, virgin female (23). At 10 d postinjury, naive dTBI animals had similar levels of baseline courtship as naive shams, indicating that injured animals were able to normally process and integrate the sensory cues required for innate courtship behavior (Fig. 2*A*). As expected, trained sham flies had a robust suppression of courtship activity upon subsequent exposure to a virgin female; however, trained dTBI flies showed impaired courtship suppression, with the courtship index being more than twice that of sham (sham trained: 0.15 ± 0.04 SEM; severe dTBI trained: 0.34 ± 0.06 SEM) (Fig. 2*A*). This indicates that, while dTBI animals retained the ability to learn, they

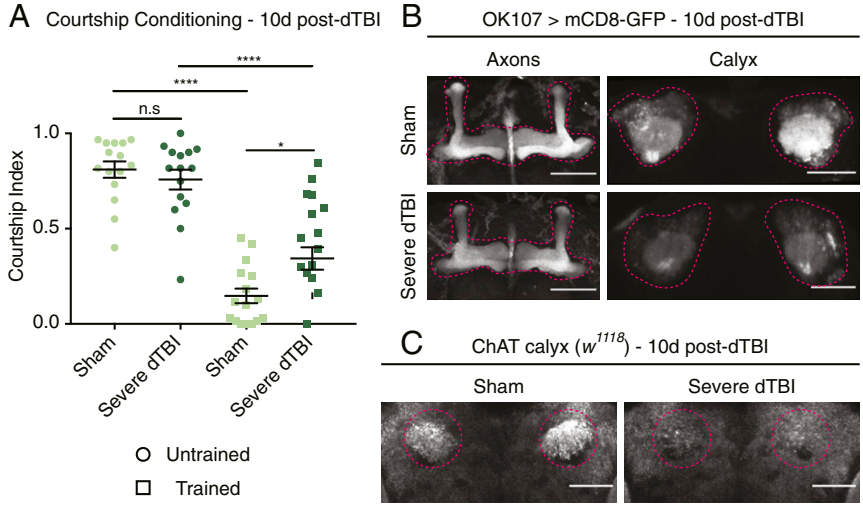

Fig. 2. Long-term neuronal and behavioral deficits in severe dTBI animals. (*A*) Severe dTBI leads to long-term cognitive decline in a paradigm of courtship conditioning. Sham and dTBI flies were either untrained or underwent a 1-h training session with a premated mature female. The flies were then immediately tested for recall of the courtship conditioning. Mean ± SEM. Number of animals: Sham (untrained), 15; Severe dTBI (untrained), 15; Sham (trained), 16; Severe dTBI (trained), 15. Genotype: Canton-S male. (*B*) Severe dTBI causes deterioration of the MB calyx at 10 d postinjury. (Scale bars: 50 μm.) Red dotted lines outline MB axonal lobes and calyx. Number of brains scored for axonal lobes: Sham, 13; Severe dTBI, 11. Number of calyces scored: Sham, 24; Severe dTBI, 20. Genotype: *UAS-mCD8-GFP/+; OK107-GAL4/+* male. (*C*) Severe dTBI causes loss of ChAT immunostaining in the MB calyx compared to sham at 10 d postinjury. (Scale bars: 100 μm.) Red dotted lines outline the ChAT immunostaining in the MB calyx. Number of calyces scored, 20 per group. Genotype: w^{1118} male. Statistics: (*A*) one-way ANOVA with Tukey's test. $^{*}P < 0.05$, $^{****}P < 0.0001$, n.s. not significant.

performed poorly in their ability to modify their behavior, suggestive of cognitive decline.

To examine whether there were any neuroanatomical indicators of cognitive decline, we examined the mushroom bodies (MBs), which are bilateral brain structures required for olfactory learning and memory (24), analogous to the hippocampus in mammals. The axonal projections of the intrinsic Kenyon cells form the lobes, which are the main output sites. The dendrites receive input from olfactory projection neurons in the calyx, making it an important site for processing olfactory information in the context of learned behaviors (25). To examine the MB, we expressed a membrane-tethered form of GFP (UAS-mCD8-GFP) using MB-specific GAL4 lines (OK107-GAL4 and 238Y-GAL4). At 10 d postinjury, labeling of the MB calyx was dramatically reduced in the dTBI brains with both drivers (Fig. 2*B* and *SI Appendix*, Fig. S3*A*). Control experiments (see below) ruled out compromise of the GAL4-UAS system with dTBI.

Acetylcholine is a key neurotransmitter of the Kenyon cells, and memory-relevant output synapses of the MB are cholinergic (25). The cholinergic neurons were therefore visualized by immunostaining for choline acetyltransferase (ChAT). Although there was no striking distinction in ChAT expression between sham and dTBI when observing the whole brain at 10 d postinjury (*SI Appendix*, Fig. S3*B*), close examination of the posteriormost layers showed that the dTBI brains had strikingly reduced immunoreactivity to ChAT in the calyx of the MB (Fig. 2*C*). This was a later onset effect because immunostaining for ChAT at 3 d postinjury showed no significant differences (*SI Appendix*, Fig. S3 *C* and *D*). The observed deterioration appeared specific to cholinergic neurons of the MB, and not a general effect across different neurotransmitter systems, as dopaminergic neuronal projections in severely injured brains at 10 d were similar to sham brains (*SI Appendix*, Fig. S3*E*). This also indicated that that GAL4-UAS expression system was functioning normally at 10 d after severe dTBI.

Overall, these results demonstrated that animals subject to severe dTBI have long-term structural effects on the calyx and cholinergic neurons of the MB; this may contribute to their deficiencies in experience-dependent modification of courtship behavior.

Severe dTBI Disrupts Glial Morphology and Function. The brain's response to injury typically involves the activation of resident glial cells to initiate inflammatory cascades, phagocytose dying cells, and form scar tissue to encapsulate damaged areas (26). To determine whether there was a glial contribution to the dTBI response, we examined three major glial subtypes—astrocytes, ensheathing glia, and subperineural glia (SPG). Astrocytes buffer extracellular calcium and provide neurotransmitter and ionic homeostasis (27). At 1 d postinjury, astrocytes were found to have relatively normal morphology (Fig. 3*A* and *SI Appendix*, Fig. S4*A*). However, at 10 d postinjury, the astrocytic labeling was markedly disrupted in dTBI animals, particularly in the antennal lobes (Fig. 3*A* and *SI Appendix*, Fig. S4*A*), suggesting that astrocytic morphology is compromised in the long term after dTBI. SPG maintain a contiguous BBB around the surface of the brain, to tightly regulate transport of nutrients and metabolites (28). Examination of the SPG layer revealed no impairments in the physical appearance of the barrier in dTBI animals either at 1 d or 10 d postinjury (*SI Appendix*, Fig. S4*B*). To assess the functional integrity of the BBB, we injected the flies with tetramethylrhodamine (TMR) conjugated dextran (molecular weight 10 kDa). The dye accumulates along the surface of brains with an intact barrier; by contrast, the dye penetrates into brains with a defective barrier (29). At 1 d postinjury, all sham brains had excluded the dye while the dTBI brains displayed significant dye intrusion into the brain parenchyma (Fig. 3*B* and *SI Appendix*, Fig. S4*C*). By 10 d postinjury, the injured animals had recovered functional BBB integrity, with all of the brains excluding the dye (Fig. 3*B* and *SI Appendix*, Fig. S4*C*). These findings indicate a transient breakdown of the BBB with severe dTBI.

Ensheathing or "wrapping" glia are the resident phagocytes of the fly nervous system (27). At 1 d postinjury, the normal wrapping morphology of the ensheathing glia (labeled with the GMR83E12 driver) was highly disorganized (*SI Appendix*, Fig. S5*A*), especially in the antennal lobes (Fig. 3*C*). A second ensheathing glial driver (MZ0709) revealed a similar disorganization of processes in the antennal lobe, as well as the optic lobe (*SI Appendix*, Fig. S5*B*). We probed the functional state of the ensheathing glia by assessing their well-characterized ability to clear debris after axotomy of the olfactory receptor neurons (ORNs) (30, 31). At 1 d post-dTBI, the third antennal segments of sham and dTBI flies were removed, causing axotomy of the ORNs. By 1 d postaxotomy, most of the axonal tracts labeled by the OR22a driver had been cleared away in the sham, but the GFP intensity in the dTBI brains was 1.3-fold higher, indicating slower clearance of debris (Fig. 3*D*). Without axotomy, there was no effect of dTBI alone on the morphology of the ORN axons (*SI Appendix*, Fig. S5*C*). By 10 d postinjury, the ensheathing glia had recovered morphologically (Fig. 3*C* and *SI Appendix*, Fig. S5*D*), and their functional activity was also restored: The clearance of debris after axotomy of the ORNs at 10 d was not significantly different between sham and dTBI flies (Fig. 3*D* and *SI Appendix*, Fig. S5*E*).

These data indicate that there is a short-term functional deterioration of the glial cells involved in the BBB and in debris clearance after severe dTBI; this is a transient effect that is largely resolved by 10 d. By contrast, astrocytic glial morphology becomes affected only by 10 d postinjury.

Cellular Stress Response Systems Are Activated Acutely in Response to dTBI. The pathophysiology of TBI is associated with the activation of several secondary cellular injury mechanisms (9). We evaluated a number of these mechanisms to gain an understanding of the molecular pathways activated upon dTBI. Oxidative stress after TBI causes neuronal dysfunction, and an increase in antioxidant enzymes such as glutathione S transferases (Gst) can help protect cells from damage by free radicals (32). We assessed this response in dTBI using a reporter construct that expresses GFP under the control of the upstream genomic sequence of the GstD1 gene (GstD-GFP) (33). Severe dTBI induced a 1.6-fold increase in GFP protein at 1 d postinjury, and a 1.9-fold increase at 3 d postinjury, compared to sham (Fig. 4*A*). Levels of GstD-GFP returned to baseline by 5 d postinjury and remained at baseline through 10 d (Fig. 4*A*). These data indicate an acute and transient antioxidant response to dTBI. To determine the localization of the response, dissected brains of injured animals were examined at 1 d postinjury. The baseline expression in sham brains was restricted to the central brain while the expression upon dTBI was widespread and extended to the optic lobes, and was increased in the antennal lobes (Fig. 4*B*).

As a consequence of cellular stress, proteins may become irreparably damaged or misfolded, necessitating removal and degradation. To assess this response, we followed a reporter for proteasome function (GFP fused to a CL1 degradation signal) (34) after dTBI. At 1 d and 3 d postinjury, GFP levels in dTBI heads were reduced to 50% of sham levels, indicating enhanced proteasome function (Fig. 4*C*). By 5 d and through 10 d postinjury, proteasome activity as reflected by the reporter had returned to baseline (Fig. 4*C*). To visualize clearance through the lysosomal pathway, we assessed the brains of sham and severely injured flies for acidified compartments using LysoTracker. At 1 d postinjury, there was a robust increase in the formation of LysoTracker-positive puncta in injured brains (sham: 1.9 ± 0.47 SEM; severe dTBI: 36.43 ± 4.9 SEM) (Fig. 4*D*). These puncta were largely

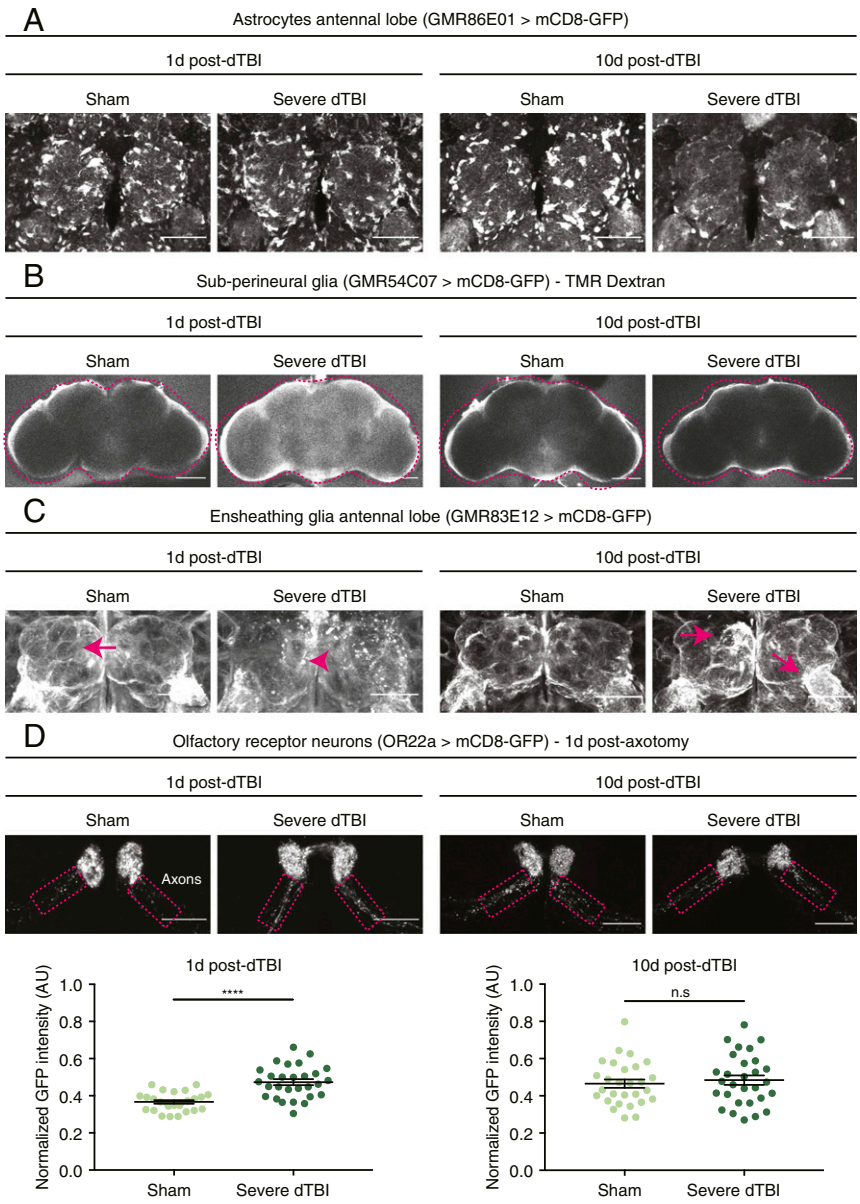

Fig. 3. Severe dTBI disrupts glial morphology and function. (*A*) Astrocytic morphology in the antennal lobe visualized by mCD8-GFP is unaffected by severe dTBI at 1 d, but is disrupted at 10 d postinjury. See *SI Appendix*, Fig. S4*A* for entire brains (Scale bars: 50 μm.) Number of antennal lobes scored for 1 d: Sham, 14; Severe dTBI, 15. For 10 d: Sham, 15; Severe dTBI, 11. Genotype: *UAS-mCD8-GFP/+; GMR86E01-GAL4/+* male. (*B*) Severe dTBI causes intrusion of injected TMR dextran dye into the brain, indicating a leaky BBB at 1 d, but not at 10 d postinjury. (Scale bars: 100 μm.) Red dotted lines outline the brain. Number of brains scored for 1 d: Sham, 13; Severe dTBI, 13. For 10 d: Sham, 8; Severe dTBI, 9. Genotype: *UAS-mCD8-GFP/+; R54C07-GAL4/+* male. (*C*) Ensheathing glia expressing mCD8-GFP in sham brains have defined wrapping morphology around antennal lobe glomeruli (arrow) that is absent in severe dTBI brains at 1 d postinjury. Instead, several dTBI brains have fluorescent puncta in that region (arrowhead). At 10 d postinjury, wrapping morphology is normal with thickened membranes around the antennal lobe (arrows) in dTBI animals. See *SI Appendix*, Fig. S5 *A* and *D* for entire brains (Scale bars: 50 μm.) Number of antennal lobes scored for 1 d: Sham, 15; Severe dTBI, 12. For 10 d: 14 per group. Genotype: *UAS-mCD8-GFP/+; GMR83E12-GAL4/+* male. (*D*) Clearance of axotomized OR22a-expressing axons labeled with mCD8-GFP is slower in severe dTBI brains at 1 d postinjury, and normal at 10 d postinjury. Third antennal segments of sham and dTBI flies were surgically removed at 1 d or 10 d post-dTBI and examined for debris clearance at 1 d postaxotomy. Total GFP intensity postaxotomy was normalized to nonaxotomized fluorescence intensity (*SI Appendix*, Fig. S5 *C* and *E*) (Scale bars: 25 μm.) Mean ± SEM. Number of axonal tracts scored for 1 d: Sham, 26; Severe dTBI, 28. For 10 d: Sham, 28; Severe dTBI, 29. Genotype: *UAS-mCD8-GFP/+; OR22a-GAL4/Sb* male. Quantification of total fluorescence intensity was done for the areas outlined in red dotted lines for *D* (AU, arbitrary units). Statistics: (*D*) Unpaired two-tailed *t* test. $^{****}P < 0.0001$, n.s., not significant.

localized to the antennal and optic lobes and persisted until 3 d postinjury (*SI Appendix*, Fig. S6*A*). By 10 d, the number of puncta had returned to baseline (Fig. 4*D*). We examined whether LysoTracker puncta were present in other injury severities at 1 d: Moderate dTBI led to increased puncta, but mild dTBI did not elicit a response (*SI Appendix*, Fig. S6*B*).

Stress, including injuries like TBI, also activates molecular chaperones, which help refold or clear impacted proteins. The stress-induced Hsp70 family of chaperones in particular is an important responder, preventing protein aggregation and assisting in the protein folding process, as well as targeting misfolded proteins for degradation via the proteasome (35). We

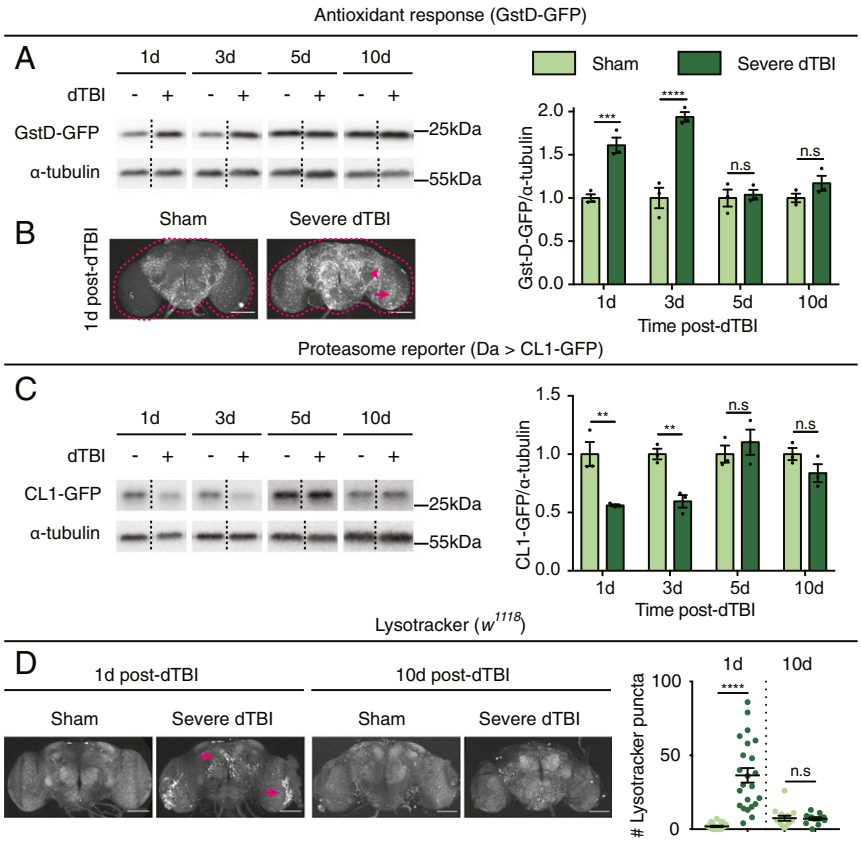

Fig. 4. Stress response systems are active acutely but not chronically after severe dTBI. (*A*) GstD-GFP reporter activity indicative of oxidative stress is increased in severe dTBI animals acutely but not chronically after injury. Mean ± SEM, three biological replicates of head tissue per group. (*B*) The GstD-GFP reporter increase at 1 d postinjury is enriched in the optic lobe (arrow) and antennal lobe (arrowhead) (Scale bars: 100 μm). Red dotted lines outline the brain. Number of brains scored: Sham, 12; Severe dTBI, 11. Genotypes for *A* and *B*: *GstD-GFP* male. (*C*) A CL1-GFP reporter indicates acute activation of the proteasomal system upon severe dTBI, which returns to baseline by 5 d postinjury. Mean ± SEM, three biological replicates of head tissue per group. Genotype: *Da-GAL4/UAS-CL1-GFP* male. (*D*) LysoTracker staining of sham and severe dTBI animals shows increased acidification of lysosomes (arrows) in dTBI animals at 1 d, but not 10 d postinjury (Scale bars: 100 μm.) Mean ± SEM. Number of brains scored for 1 d: Sham, 21; Severe dTBI, 23. For 10 d: 14 per group. Genotype: w^{1118} male. Uncropped images of Western blots are found in *SI Appendix*, Fig. S7. Statistics: (*A* and *C*) two-way ANOVA with Sidak's test (dTBI compared to corresponding sham at each time point). (*D*) Unpaired two-tailed *t* test. $^{**}P < 0.01$, $^{***}P < 0.001$, $^{****}P < 0.0001$; n.s., not significant.

assessed to what extent dTBI brains launched a stress response by determining levels of stress-induced Hsp70. Upon severe dTBI, there was a robust 3.7-fold increase in Hsp70 protein within 3 h that was sustained at 1 d postinjury (Fig. 5*A*). As with the other molecular responses, the levels of Hsp70 had returned to baseline by 5 d (Fig. 5*A*).

Taken together, these findings indicate that the severely injured brain mounts a robust and acute protective response to the trauma that becomes attenuated by 5 d.

The Stress Response Protects from dTBI. Up-regulation of molecular chaperones is protective in a number of neurodegenerative conditions (36). Thus, we considered whether activating the stress response prior to the dTBI either through genetic means or environmental manipulations would be beneficial. We first used a fly line with an additional genomic copy of the *Hsf* gene (37)—the transcription factor that induces the stress response—in the control w^{1118} background. When subjected to severe dTBI, animals with added *Hsf* showed an extended life span (median life span extended by 7 d; maximum life span by 13 d) (Fig. 5*B*). This protection included preservation of brain integrity: Animals with added *Hsf* had a 40% reduction in the vacuole area throughout the brain at 1 d postinjury (Fig. 5*C*).

Given that genomic enhancement of *Hsf* could mitigate dTBI, we then investigated whether an acute boost of the endogenous stress response by transient heat shock of the animals could also confer protection from dTBI. We subjected normal w^{1118} animals to a mild heat shock (37 °C, 30 min) 1 h prior to severe dTBI. The effect of the pretreatment was similar to chronic genomic up-regulation of *Hsf* (median life span extended by 6 d; maximum life span by 14 d; vacuole area reduced by 40%) (Fig. 5 *D* and *E*). Importantly, the protection provided by augmentation of the stress response shifted the life span and vacuole phenotype of the severe dTBI animals to be comparable to a moderate dTBI.

These data indicate that enhancing the stress response through genetic or environmental means is protective against the deleterious consequences to life span and brain vacuolization upon severe dTBI.

Discussion

We report the development and detailed characterization of a tunable, head-specific paradigm for TBI in *Drosophila*, called dTBI. The paradigm inflicts a reproducible, precise trauma to the fly head, with an adjustable threshold for three different severities of head injury: "mild" (35%), "moderate" (40%), and "severe" (45%) head compression (*SI Appendix*, Table S1). The

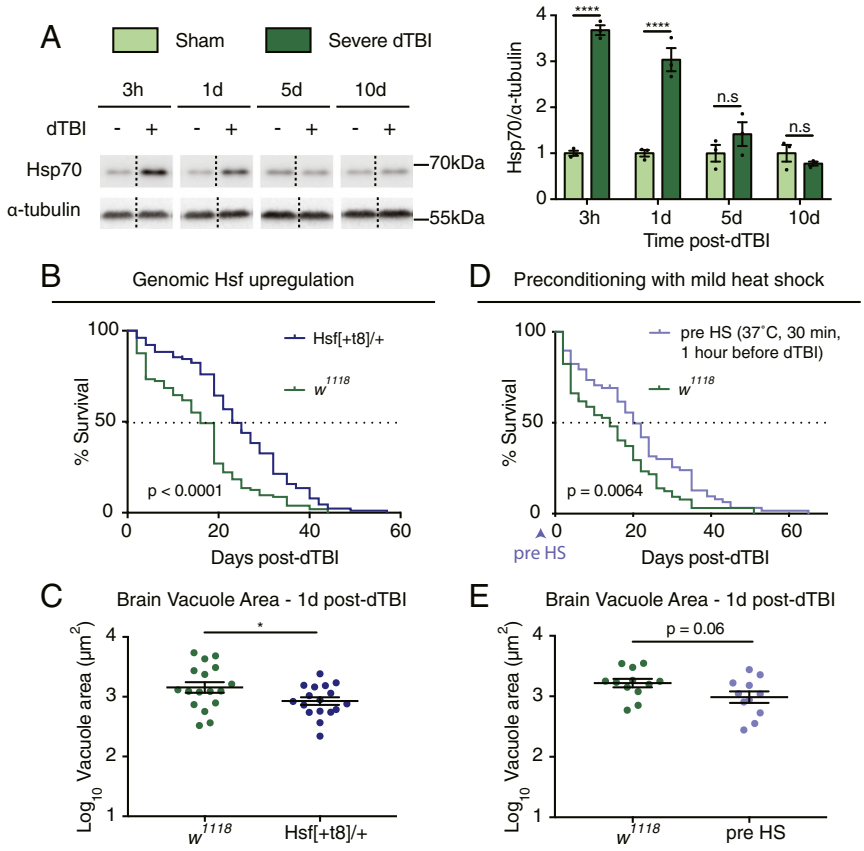

Fig. 5. Augmenting the stress response protects against severe dTBI. (*A*) Hsp70 is increased within 3 h upon severe dTBI and returns to baseline by 5 d postinjury. Mean ± SEM, three biological replicates of head tissue per group. Genotype: w^{1118} male. (*B*) An added genomic copy of the *Hsf* gene in the w^{1118} background extends median life span by 7 d after severe dTBI. Number of animals, 103 flies per group. (*C*) Added genomic *Hsf* mitigates formation of brain vacuoles at 1 d postinjury ($\log_{10}$ of vacuole area [μm^2]). Mean ± SEM. Number of brains scored: 17 per group. Genotypes for *B* and *C*: w^{1118} and w^{1118}*; Hsf[+t8]/+* male. (*D*) Preconditioning flies with a mild heat shock (pre-HS) (37 °C, 30 min) 1 h before severe dTBI extends median life span by 6 d. Number of animals, 70 flies per group. (*E*) Mild heat shock preconditioning mitigates formation of brain vacuoles at 1 d postinjury ($\log_{10}$ of vacuole area [μm^2]). Mean ± SEM. Number of brains scored: Sham, 12; Severe dTBI, 11. Genotypes for *D* and *E*: w^{1118} male. Uncropped images of Western blots found in *SI Appendix*, Fig. S7. Statistics: (*A*) Two-way ANOVA with Sidak's test (dTBI compared to corresponding sham at each time point). (*B* and *D*) Log-rank test. (*C* and *E*) Unpaired two-tailed *t* test. **P* < 0.05, *****P* < 0.0001.

brain injury is inflicted by rapidly compressing the fly head between two solid surfaces, resulting in the deformation of the brain. This compression injury resembles the rapid deformation of the human brain during a closed head TBI, which causes axons to distort and shear, resulting in diffuse axonal injury (DAI) (38). Our extensive characterization shows that dTBI causes immediate and long-lasting neurological deficits and transient functional deficits in glial cells and promotes an acute cellular stress response. Deficits in righting reflex, climbing, life span, and brain vacuolization scale with injury severity (*SI Appendix*, Table S1). We observe that many histological hallmarks of injury (disruption of ensheathing glial processes, GstD-GFP activation, LysoTracker puncta) appear primarily in the upper layers of the cortex around the antennal lobe and optic lobes. It is likely that the upper cortex is most affected as it is closest to the site of impact of the piezoelectric plate. However, vacuolization of the neuropil in deeper regions of the brain indicates that degeneration is progressing throughout the brain as a consequence of dTBI.

Many of the phenotypes described with this model are observed with human TBI and follow similar timescales. Severity-dependent loss of consciousness in humans occurs immediately following TBI (39, 40), as a consequence of complex ionic and metabolic changes (8). Such changes render the brain more excitable, causing posttraumatic seizures most commonly within the first few days after injury (41); in the dTBI model, behaviors reminiscent of seizures occur most frequently within the first 30 min of injury. The primary injury and resultant secondary molecular cascades cause endothelial cell tight junctions to transiently break down, increasing the permeability of the BBB in the first few hours after TBI (42, 43). Reactive astrogliosis is an early hallmark of injury and is marked by glial fibrillary acidic protein, and the response includes repair of the BBB, phagocytosis of synapses, and clearance of debris (44). However, invertebrates do not possess glial fibrillary acidic protein, and previous studies of axon transection in *Drosophila* also show no immediate astrocytic response to injury (30, 45). In the fly, ensheathing glia express key components of the phagocytic machinery and respond morphologically to injury to clear neuronal debris (30). Fly astrocytes modulate synaptic signaling and are metabolically coupled with neurons (46) and thus might degenerate along with neurons in response to dTBI. Other secondary molecular events include an increase in oxidative stress, resultant of an imbalance between the production of reactive oxygen species and its degradation through antioxidant systems (32). With dTBI, there is an increase in the GstD-GFP marker of oxidative stress within 1 d of injury which is sustained till at least 3 d, in agreement with data from a rat model of TBI, where

markers of oxidative stress appeared within 3 h of injury, were sustained till 3 d, and returned to baseline by 4 d post-TBI (47). Acute alterations in proteasomal function (48), chaperone activation (49, 50), and the neuroprotective effects of the protein degradation systems (51) have been reported in mammalian experimental models of TBI. These secondary molecular pathways instigate brain-wide cell death that has been visualized in TBI models (52, 53), with maximum degeneration between 1 d and 7 d post-TBI (54). Neurodegeneration continues throughout the postinjury phase, with brain atrophy rates of up to 5% per year (55). This chronic neurodegeneration causes behavioral changes (56), loss of motor coordination (57), and cognitive deficits (58) and is thought to accelerate the biological aging process (59). In the dTBI model, necrosis is observed at 1 d postinjury, and brain vacuolization progresses over time, with the animals showing early and persistent loss of locomotor ability as well cognitive dysfunction at 10 d postinjury.

Elevation of the stress-induced chaperone Hsp70 is one of the most robust changes seen in the dTBI model. Human patient TBI samples show that the inducible form of HSP70 increases following TBI, with the highest change in protein expression occurring at 12 to 20 h postinjury (49, 50). Importantly, in rodent models of TBI, pharmacological or genetic induction of HSP70 improves physiological outcomes (lesion size, neuronal cell death) while animals lacking HSP70 have significantly worsened neurological outcomes (60–62). Global preconditioning of the animal with low level stressors, such as ischemia, hypoxia, hypothermia (63), and chronic hyperthermia (64), has been shown to confer protection against a wide range of injuries, including TBI. Our findings extend these data to demonstrate that chronic genetic up-regulation of Hsf or a transient activation of the entire repertoire of the stress response immediately prior to brain injury is beneficial. An important consequence of TBI is the long-term accumulation of proteins in neuropathologic aggregates and the increased risk of neurodegenerative disorders, including CTE and Alzheimer's disease (65). Several chaperones, namely HSP70 (and its cochaperone HSP40), HSP90, and HSP27, have been identified as important modulators of neurotoxicity, reducing the aggregation of polyQ (66–68), tau (69), amyloid-β (70, 71), and α-synuclein (72–74) proteins. In addition to their proteostatic properties, chaperones also play an important role in the clearance of misfolded proteins through the proteasome and chaperone-mediated autophagy, and the inhibition of signaling pathways that lead to apoptosis. Although many of the ameliorative properties of chaperones in TBI have focused on HSP70, evidence from the study of neurodegenerative diseases suggests that the coordinated increase of multiple chaperones could exert protective influences.

These physiological and molecular similarities of the dTBI response to the established mammalian models demonstrate that many injury mechanisms are conserved between *Drosophila* and mammals, and that the fly is a valuable addition to the array of tools in TBI research.

This dTBI paradigm represents a complement to the current trauma approaches (17, 19) for studying TBI using *Drosophila*. The dTBI effect on life span is a robust, sensitive assay and is associated with severity of brain degeneration. The life span assay can statistically distinguish between injury severities and be used as a readout for defining postinjury outcome. Thus, genetic screens can be readily performed with this apparatus for identification of genetic and environmental modifiers of TBI-related phenotypes. By integrating mammalian findings and approaches, this and other fly models will advance our understanding of the complex pathophysiology of TBI and provide the foundation for the development of therapeutic interventions.

Materials and Methods

Detailed methods are described in *SI Appendix*.

***Drosophila* Work.** All *Drosophila* strains were maintained on standard cornmeal-molasses medium at 26 °C in light/dark controlled incubators. Adult 3-d-old male flies were used for all TBI experiments. A full list of fly lines used is in *SI Appendix*, Table S2.

Construction of the dTBI Device. Custom Heisenberg fly collars were used to restrain flies and built based on specifications from previous publications (21) with a minor modification to narrow the gap. The dTBI device was assembled, calibrated, and tested in the laboratory (*SI Appendix*, Fig. S1*A*) (75). The main components of the device are readily available and include a piezoelectric actuator (q220-a4-203yb; piezo.com), an Arduino microcontroller-based system (digikey.com, 1050-1024-ND; A000066, Arduino), and a power amplifier (EVB-304; piezo.com). The microcontroller system controls a relay switch (Z1228-ND, digikey.com; G6L-1P DC5, Omron Electronics Inc.-EMC Division) that supplies a transient voltage to the power amplifier. The amplified voltage causes the piezoelectric actuator to bend rapidly within 250 ms. This bending results in a linear displacement of the actuator and subsequent compression of the fly head against the metal plates of the Heisenberg collar. Other components of the circuit include a push-button to complete the circuit (amazon.com ASIN B0772KYPPM; Ocrtech), a potentiometer to set the required voltage (amazon.com ASIN B017LB2YCM; a15082600ux0077, Uxcell), a buck converter to step down the voltage to the relay switch (amazon.com ASIN B008BHAOQO; 3-01-0076, UPC 797698770222, RioRand), and a digital voltmeter display (amazon.com ASIN B00YALV0NG, 3B002x5; Bayite).

Histology. Horizontal paraffin sections were processed as described (76). Immunohistochemistry (77), LysoTracker (78), propidium iodide (79), BBB functional analysis (29), and axon injury assays (31) were performed on whole mount brains as described previously.

Western Blotting. Western blotting was performed on head tissue as previously described (76).

Data Availability. All data associated with the manuscript are provided within the manuscript; additional detailed information that is required to assemble and use the dTBI device is publicly accessible at Protocol Exchange (http://dx.doi.org/10.21203/rs.3.pex-949/v1) (75).

ACKNOWLEDGMENTS. We thank Marc Freeman, Dirk Bohmann, and Paul Taylor for sharing fly stocks. We thank Alexandra Perlegos, Ananth Srinivasan, and past members of the N.M.B. laboratory for critical input. We thank Michael Suplick and Fred Letterio (University of Pennsylvania Machine Shop) for making and modifying the fly collars. This work was supported by a predoctoral Howard Hughes Medical Institute fellowship (to J.S.); and funding from NIH Grant R35-NS097275 (to N.M.B.), the Paul G. Allen Frontiers group, and NIH Grant NS088176 (to D.F.M.).

1. M. C. Dewan *et al.*, Estimating the global incidence of traumatic brain injury. *J. Neurosurg.*, 1–18 (2018).
2. C. A. Taylor, J. M. Bell, M. J. Breiding, L. Xu, Traumatic brain injury-related emergency department visits, hospitalizations, and deaths–United States, 2007 and 2013. *MMWR Surveill. Summ.* **66**, 1–16 (2017).
3. D. H. Daneshvar, L. E. Goldstein, P. T. Kiernan, T. D. Stein, A. C. McKee, Post-traumatic neurodegeneration and chronic traumatic encephalopathy. *Mol. Cell. Neurosci.* **66**, 81–90 (2015).
4. A. Chodobski, B. J. Zink, J. Szmydynger-Chodobska, Blood-brain barrier pathophysiology in traumatic brain injury. *Transl. Stroke Res.* **2**, 492–516 (2011).
5. J.-H. H. Yi, A. S. Hazell, Excitotoxic mechanisms and the role of astrocytic glutamate transporters in traumatic brain injury. *Neurochem. Int.* **48**, 394–403 (2006).
6. K. R. Walker, G. Tesco, Molecular mechanisms of cognitive dysfunction following traumatic brain injury. *Front. Aging Neurosci.* **5**, 29 (2013).
7. K. Blennow *et al.*, Traumatic brain injuries. *Nat. Rev. Dis. Primers* **2**, 16084 (2016).
8. C. C. Giza, D. A. Hovda, The new neurometabolic cascade of concussion. *Neurosurgery* **75** (suppl. 4), S24–S33 (2014).
9. C. Werner, K. Engelhard, Pathophysiology of traumatic brain injury. *Br. J. Anaesth.* **99**, 4–9 (2007).
10. K. Blennow, J. Hardy, H. Zetterberg, The neuropathology and neurobiology of traumatic brain injury. *Neuron* **76**, 886–899 (2012).
11. S. Shively, A. I. Scher, D. P. Perl, R. Diaz-Arrastia, Dementia resulting from traumatic brain injury: What is the pathology? *Arch. Neurol.* **69**, 1245–1251 (2012).
12. A. I. R. Maas, B. Roozenbeek, G. T. Manley, Clinical trials in traumatic brain injury: Past experience and current developments. *Neurotherapeutics* **7**, 115–126 (2010).

13. U. B. Pandey, C. D. Nichols, Human disease models in Drosophila melanogaster and the role of the fly in therapeutic drug discovery. *Pharmacol. Rev.* **63**, 411–436 (2011).
14. L. McGurk, A. Berson, N. M. Bonini, Drosophila as an in vivo model for human neurodegenerative disease. *Genetics* **201**, 377–402 (2015).
15. A. H. Brand, N. Perrimon, Targeted gene expression as a means of altering cell fates and generating dominant phenotypes. *Development* **118**, 401–415 (1993).
16. T. Osterwalder, K. S. Yoon, B. H. White, H. Keshishian, A conditional tissue-specific transgene expression system using inducible GAL4. *Proc. Natl. Acad. Sci. U.S.A.* **98**, 12596–12601 (2001).
17. R. J. Katzenberger *et al*., A Drosophila model of closed head traumatic brain injury. *Proc. Natl. Acad. Sci. U.S.A.* **110**, E4152–E4159 (2013).
18. R. J. Katzenberger *et al*., Death following traumatic brain injury in Drosophila is associated with intestinal barrier dysfunction. *eLife* **4**, e04790 (2015).
19. A. Barekat *et al*., Using Drosophila as an integrated model to study mild repetitive traumatic brain injury. *Sci. Rep.* **6**, 25252 (2016).
20. M. Sun, L. L. Chen, A novel method to model chronic traumatic encephalopathy in Drosophila. *J. Vis. Exp.*, 55602 (2017).
21. M. Heisenberg, K. Böhl, Isolation of anatomical brain mutants of Drosophila by histological means. *Z. Naturforsch. C* **34**, 143–147 (1979).
22. X. Zhang, Y. Chen, L. W. Jenkins, P. M. Kochanek, R. S. Clark, Bench-to-bedside review: Apoptosis/programmed cell death triggered by traumatic brain injury. *Crit. Care* **9**, 66–75 (2005).
23. R. W. Siegel, J. C. Hall, Conditioned responses in courtship behavior of normal and mutant Drosophila. *Proc. Natl. Acad. Sci. U.S.A.* **76**, 3430–3434 (1979).
24. K. Yasuyama, I. A. Meinertzhagen, F. W. Schürmann, Synaptic organization of the mushroom body calyx in Drosophila melanogaster. *J. Comp. Neurol.* **445**, 211–226 (2002).
25. O. Barnstedt *et al*., Memory-relevant mushroom body output synapses are cholinergic. *Neuron* **89**, 1237–1247 (2016).
26. I. P. Karve, J. M. Taylor, P. J. Crack, The contribution of astrocytes and microglia to traumatic brain injury. *Br. J. Pharmacol.* **173**, 692–702 (2016).
27. M. R. Freeman, Drosophila central nervous system Glia. *Cold Spring Harb. Perspect. Biol.* **7**, a020552 (2015).
28. S. J. Hindle, R. J. Bainton, Barrier mechanisms in the Drosophila blood-brain barrier. *Front. Neurosci.* **8**, 414 (2014).
29. R. L. Pinsonneault, N. Mayer, F. Mayer, N. Tegegn, R. J. Bainton, Novel models for studying the blood-brain and blood-eye barriers in Drosophila. *Methods Mol. Biol.* **686**, 357–369 (2011).
30. J. Doherty, M. A. Logan, O. E. Taşdemir, M. R. Freeman, Ensheathing glia function as phagocytes in the adult Drosophila brain. *J. Neurosci.* **29**, 4768–4781 (2009).
31. J. M. MacDonald *et al*., The Drosophila cell corpse engulfment receptor Draper mediates glial clearance of severed axons. *Neuron* **50**, 869–881 (2006).
32. A. Rodríguez-Rodríguez, J. J. Egea-Guerrero, F. Murillo-Cabezas, A. Carrillo-Vico, Oxidative stress in traumatic brain injury. *Curr. Med. Chem.* **21**, 1201–1211 (2014).
33. G. P. Sykiotis, D. Bohmann, Keap1/Nrf2 signaling regulates oxidative stress tolerance and lifespan in Drosophila. *Dev. Cell* **14**, 76–85 (2008).
34. U. B. Pandey *et al*., HDAC6 rescues neurodegeneration and provides an essential link between autophagy and the UPS. *Nature* **447**, 859–863 (2007).
35. L. Petrucelli *et al*., CHIP and Hsp70 regulate tau ubiquitination, degradation and aggregation. *Hum. Mol. Genet.* **13**, 703–714 (2004).
36. I. Lindberg *et al*., Chaperones in neurodegeneration. *J. Neurosci.* **35**, 13853–13859 (2015).
37. P. Jedlicka, M. A. Mortin, C. Wu, Multiple functions of Drosophila heat shock transcription factor in vivo. *EMBO J.* **16**, 2452–2462 (1997).
38. V. E. Johnson, W. Stewart, D. H. Smith, Axonal pathology in traumatic brain injury. *Exp. Neurol.* **246**, 35–43 (2013).
39. B. J. Blyth, J. J. Bazarian, Traumatic alterations in consciousness: Traumatic brain injury. *Emerg. Med. Clin. North Am.* **28**, 571–594 (2010).
40. D. H. Smith, D. F. Meaney, W. H. Shull, Diffuse axonal injury in head trauma. *J. Head Trauma Rehabil.* **18**, 307–316 (2003).
41. I. Asikainen, M. Kaste, S. Sarna, Early and late posttraumatic seizures in traumatic brain injury rehabilitation patients: Brain injury factors causing late seizures and influence of seizures on long-term outcome. *Epilepsia* **40**, 584–589 (1999).
42. V. N. Bharadwaj, J. Lifshitz, P. D. Adelson, V. D. Kodibagkar, S. E. Stabenfeldt, Temporal assessment of nanoparticle accumulation after experimental brain injury: Effect of particle size. *Sci. Rep.* **6**, 29988 (2016).
43. B. J. Kelley, J. Lifshitz, J. T. Povlishock, Neuroinflammatory responses after experimental diffuse traumatic brain injury. *J. Neuropathol. Exp. Neurol.* **66**, 989–1001 (2007).
44. S. A. Liddelow, B. A. Barres, Reactive astrocytes: Production, function, and therapeutic potential. *Immunity* **46**, 957–967 (2017).
45. M. D. Purice *et al*., A novel *Drosophila* injury model reveals severed axons are cleared through a Draper/MMP-1 signaling cascade. *eLife* **6**, e23611 (2017).
46. A. Volkenhoff *et al*., Glial glycolysis is essential for neuronal survival in Drosophila. *Cell Metab.* **22**, 437–447 (2015).
47. M. A. Ansari, K. N. Roberts, S. W. Scheff, A time course of contusion-induced oxidative stress and synaptic proteins in cortex in a rat model of TBI. *J. Neurotrauma* **25**, 513–526 (2008).
48. X. Yao, J. Liu, J. T. McCabe, Alterations of cerebral cortex and hippocampal proteasome subunit expression and function in a traumatic brain injury rat model. *J. Neurochem.* **104**, 353–363 (2008).
49. S. A. Dutcher, B. D. Underwood, P. D. Walker, F. G. Diaz, D. B. Michael, Patterns of heat-shock protein 70 biosynthesis following human traumatic brain injury. *J. Neurotrauma* **15**, 411–420 (1998).
50. N. A. Seidberg *et al*., Alterations in inducible 72-kDa heat shock protein and the chaperone cofactor BAG-1 in human brain after head injury. *J. Neurochem.* **84**, 514–521 (2003).
51. H. Ding *et al*., Nrf2-ARE signaling provides neuroprotection in traumatic brain injury via modulation of the ubiquitin proteasome system. *Neurochem. Int.* **111**, 32–44 (2017).
52. R. Hicks, H. Soares, D. Smith, T. McIntosh, Temporal and spatial characterization of neuronal injury following lateral fluid-percussion brain injury in the rat. *Acta Neuropathol.* **91**, 236–246 (1996).
53. S. C. Cortez, T. K. McIntosh, L. J. Noble, Experimental fluid percussion brain injury: Vascular disruption and neuronal and glial alterations. *Brain Res.* **482**, 271–282 (1989).
54. M. Sato, E. Chang, T. Igarashi, L. J. Noble, Neuronal injury and loss after traumatic brain injury: Time course and regional variability. *Brain Res.* **917**, 45–54 (2001).
55. T. C. Harris, R. de Rooij, E. Kuhl, The shrinking brain: Cerebral atrophy following traumatic brain injury. *Ann. Biomed. Eng.* **47**, 1941–1959 (2019).
56. T. W. McAllister, Neurobehavioral sequelae of traumatic brain injury: Evaluation and management. *World Psychiatry* **7**, 3–10 (2008).
57. G. Williams, M. E. Morris, A. Schache, P. R. McCrory, Incidence of gait abnormalities after traumatic brain injury. *Arch. Phys. Med. Rehabil.* **90**, 587–593 (2009).
58. D. H. Smith, V. E. Johnson, W. Stewart, Chronic neuropathologies of single and repetitive TBI: substrates of dementia? *Nat. Rev. Neurol.* **9**, 211–221 (2013).
59. J. H. Cole, R. Leech, D. J. Sharp; Alzheimer's Disease Neuroimaging Initiative, Prediction of brain age suggests accelerated atrophy after traumatic brain injury. *Ann. Neurol.* **77**, 571–581 (2015).
60. J. Y. Kim, N. Kim, Z. Zheng, J. E. Lee, M. A. Yenari, The 70 kDa heat shock protein protects against experimental traumatic brain injury. *Neurobiol. Dis.* **58**, 289–295 (2013).
61. B. Eroglu *et al*., Therapeutic inducers of the HSP70/HSP110 protect mice against traumatic brain injury. *J. Neurochem.* **130**, 626–641 (2014).
62. N. Kim, J. Y. Kim, M. A. Yenari, Pharmacological induction of the 70-kDa heat shock protein protects against brain injury. *Neuroscience* **284**, 912–919 (2015).
63. R. A. Stetler *et al*., Preconditioning provides neuroprotection in models of CNS disease: Paradigms and clinical significance. *Prog. Neurobiol.* **114**, 58–83 (2014).
64. N. A. Shein, M. Horowitz, E. Shohami, Heat acclimation: A unique model of physiologically mediated global preconditioning against traumatic brain injury. *Prog. Brain Res.* **161**, 353–363 (2007).
65. D. H. Smith, K. Uryu, K. E. Saatman, J. Q. Trojanowski, T. K. McIntosh, Protein accumulation in traumatic brain injury. *Neuromolecular Med.* **4**, 59–72 (2003).
66. C. J. Cummings *et al*., Over-expression of inducible HSP70 chaperone suppresses neuropathology and improves motor function in SCA1 mice. *Hum. Mol. Genet.* **10**, 1511–1518 (2001).
67. A. Wyttenbach *et al*., Effects of heat shock, heat shock protein 40 (HDJ-2), and proteasome inhibition on protein aggregation in cellular models of Huntington's disease. *Proc. Natl. Acad. Sci. U.S.A.* **97**, 2898–2903 (2000).
68. A. Sittler *et al*., Geldanamycin activates a heat shock response and inhibits huntingtin aggregation in a cell culture model of Huntington's disease. *Hum. Mol. Genet.* **10**, 1307–1315 (2001).
69. H. Shimura, Y. Miura-Shimura, K. S. Kosik, Binding of tau to heat shock protein 27 leads to decreased concentration of hyperphosphorylated tau and enhanced cell survival. *J. Biol. Chem.* **279**, 17957–17962 (2004).
70. J. Magrané, R. C. Smith, K. Walsh, H. W. Querfurth, Heat shock protein 70 participates in the neuroprotective response to intracellularly expressed beta-amyloid in neurons. *J. Neurosci.* **24**, 1700–1706 (2004).
71. K. Takata *et al*., Heat shock protein-90-induced microglial clearance of exogenous amyloid-beta1-42 in rat hippocampus in vivo. *Neurosci. Lett.* **344**, 87–90 (2003).
72. A. Zourlidou, M. D. Payne Smith, D. S. Latchman, HSP27 but not HSP70 has a potent protective effect against alpha-synuclein-induced cell death in mammalian neuronal cells. *J. Neurochem.* **88**, 1439–1448 (2004).
73. P. K. Auluck, H. Y. Chan, J. Q. Trojanowski, V. M. Lee, N. M. Bonini, Chaperone suppression of alpha-synuclein toxicity in a Drosophila model for Parkinson's disease. *Science* **295**, 865–868 (2002).
74. J. Klucken, Y. Shin, E. Masliah, B. T. Hyman, P. J. McLean, Hsp70 reduces alpha-synuclein aggregation and toxicity. *J. Biol. Chem.* **279**, 25497–25502 (2004).
75. J. Saikumar *et al*, dTBI: A paradigm for closed-head injury in Drosophila. *Protocol Exchange*. http://dx.doi.org/10.21203/rs.3.pex-949/v1. Deposited 21 May 2020.
76. C. Y. Chung *et al*., Aberrant activation of non-coding RNA targets of transcriptional elongation complexes contributes to TDP-43 toxicity. *Nat. Commun.* **9**, 4406 (2018).
77. D. J. Cavanaugh *et al*., Identification of a circadian output circuit for rest:activity rhythms in Drosophila. *Cell* **157**, 689–701 (2014).
78. K. J. Kinghorn *et al*., A Drosophila model of neuronopathic gaucher disease demonstrates lysosomal-autophagic defects and altered mTOR signalling and is functionally rescued by rapamycin. *J. Neurosci.* **36**, 11654–11670 (2016).
79. Y. Yang, L. Hou, Y. Li, J. Ni, L. Liu, Neuronal necrosis and spreading death in a Drosophila genetic model. *Cell Death Dis.* **4**, e723 (2013).